HHS Public Access

Author manuscript

Circ Res. Author manuscript; available in PMC 2021 July 03.

Published in final edited form as:

Circ Res. 2020 July 03; 127(2): e28–e43. doi:10.1161/CIRCRESAHA.119.316415.

ZO-1 Regulates Intercalated Disc Composition and Atrioventricular Node Conduction

Wenli Dai[1], **Rangarajan D. Nadadur**[2], **Jaclyn A. Brennan**[3], **Heather L. Smith**[1], **Kaitlyn M. Shen**[2], **Margaret Gadek**[2], **Brigitte Laforest**[4], **Mingyi Wang**[5], **Joanna Gemel**[6], **Ye Li**[1], **Jing Zhang**[5], **Bruce D. Ziman**[5], **Jiajie Yan**[7], **Xun Ai**[7], **Eric C. Beyer**[6], **Edward G. Lakata**[5], **Narayanan Kasthuri**[8], **Igor R. Efimov**[3], **Michael T. Broman**[4], **Ivan P. Moskowitz**[2], **Le Shen**[1,9,†], **Christopher R. Weber**[1,†]

[1]Pathology, University of Chicago, 5841 S. Maryland Ave., Chicago, IL 60637;

[2]Pediatrics, Pathology, and Human Genetics, University of Chicago, Chicago, IL 60637, USA;

[3]Department of Biomedical Engineering, The George Washington University, 800 22nd St NW, Washington, DC 20052;

[4]Medicine, Section of Cardiology, University of Chicago, 5841 S. Maryland Ave., Chicago, IL 60637;

[5]Laboratory of Cardiovascular Science, National Institution on Aging-NIH, BRC-9B0127 251 Bayview Blvd, Baltimore, MD 21224;

[6]Pediatrics, University of Chicago, Chicago, IL 60637, USA;

[7]Physiology and Biophysics, Rush University, 1750 West Harrison St., Chicago, IL 60612;

[8]Neurobiology, University of Chicago, 5841 S. Maryland Ave., Chicago, IL 60637;

[9]Section of Neurosurgery, Department of Surgery, University of Chicago, 5841 S. Maryland Ave., Chicago, IL 60637.

Abstract

Rationale: Zona occludens 1 (ZO-1), encoded by the Tight Junction Protein 1 (*TJP1)* gene, is a regulator of paracellular permeability in epithelia and endothelia. ZO-1 interacts with the actin cytoskeleton, gap and adherens junction proteins, and localizes to intercalated discs in cardiomyocytes. However, the contribution of ZO-1 to cardiac physiology remains poorly defined.

Objective: We aim to determine the role of ZO-1 in cardiac function.

Address correspondence to: Dr. Christopher Weber, Pathology, University of Chicago, 5841 S. Maryland Ave. Chicago, IL 60637, Tel: 708-466-1056, christopher.weber@uchospitals.edu, Dr. Le Shen, Pathology, University of Chicago, 5841 S. Maryland Ave. Chicago, IL 60637, leshen@uchicago.edu.

†These authors contributed equally to this work.

DISCLOSURES

None.

SUPPLEMENTAL MATERIALS

Online Figures I - VIII

Major Resources Table

Uncut Gel Blots

Methods and Results: Inducible cardiomyocyte-specific *Tjp1* deletion mice (*Tjp1*$^{fl/fl}$; *Myh6*$^{Cre/Esr1*}$) were generated by crossing the *Tjp1* floxed mice and *Myh6*$^{Cre/Esr1*}$ transgenic mice. Tamoxifen-induced loss of ZO-1 led to atrioventricular (AV) block without changes in heart rate, as measured by electrocardiogram (ECG) and *ex vivo* optical mapping. Mice with tamoxifen-induced conduction system specific deletion of *Tjp1* (*Tjp1*$^{fl/fl}$; *Hcn4*^{CreERt2}) developed AV block while tamoxifen-induced conduction system deletion of *Tjp1* distal to the AV node (*Tjp1*$^{fl/fl}$; *Kcne1*^{CreERt2}) did not demonstrate conduction defects. Western blot and immunostaining analyses of AV nodes showed that ZO-1 loss decreased connexin (Cx) 40 expression and intercalated disc localization. Consistent with the mouse model study, immunohistochemical staining showed that ZO-1 is abundantly expressed in the human AV node, and colocalizes with Cx40. Ventricular conduction was not altered despite decreased localization of ZO-1 and Cx43 at the ventricular intercalated disc and slightly decreased left ventricular ejection fraction, suggesting ZO-1 is differentially required for AV node and ventricular conduction.

Conclusion: ZO-1 is a key protein responsible for maintaining appropriate AV node conduction through maintaining gap junction protein localization.

Abstract

Intercalated discs, found at the ends of cardiomyocytes, provide mechanical and electrical coupling between individual cells. However, our understanding of the molecular determinants of intercalated disc structure and function remains limited. In this study, we investigated the role of ZO-1, a cytoskeletal protein that can link transmembrane proteins and cytoskeletal components to stabilize multiprotein complexes in the intercalated disc. We found that loss of ZO-1 in cardiomyocytes disrupts connexin localization at intercalated discs and results in PR prolongation and dissociation of atrial and ventricular depolarization, indicating heart block. Further, we found ZO-1 is highly expressed in the AV node compared with surrounding atrial and ventricular tissue and loss of ZO-1 leads to decreased localization of connexin 40 and coxsackie and adenovirus receptor (CAR) at AV node intercalated. This work shows ZO-1 is important for regulating AV conduction and given previous findings from connexin 40 and CAR knockout mice, we propose ZO-1, connexin 40, and CAR form a functional complex within intercalated discs to regulate AV conduction. These findings suggest a need to understand the structural-functional relationships of the connexin-ZO-1-CAR protein complex at the intercalated disc, which may lead to novel ways to relieve heart blocks in patients.

Subject Terms

Arrhythmias; Basic Science Research; Myocardial Biology; Pathophysiology

Keywords

ZO-1; *TJP1*; tight junction; intercalated disc; cardiac conduction; AV node; cardiac gap junction connexins; cardiac function; cardiac arrhythmia; atrioventricular block; intercellular junction

INTRODUCTION

ZO-1, encoded by the *TJP1* gene, is a cytoplasmic scaffolding protein critical to the function of the apical junctional complex[1–3]. Its essential function as a regulator of paracellular permeability is well recognized[2, 4]. In addition to binding to transmembrane proteins that dictate paracellular permeability[5–7], ZO-1 can bind to the actin cytoskeleton and the adherens junction component, α-catenin[5, 8–11]. Although ZO-1 is widely expressed in multiple cell types, its function has mostly been studied in epithelial and endothelial cells[4, 12, 13].

While its function in the heart remains poorly defined[14], ZO-1 is known to be enriched at the myocardial intercalated disc[15–18], which contains multiple components, including gap junctions, adherens junctions, and desmosomes[17]. ZO-1 has been shown to bind to multiple intercalated disc proteins, including Coxsackie and adenovirus receptor (CAR)[19] and gap junction proteins connexin (Cx) 35, 36, 40, 43, and 45[16, 20–23], and vinculin[24]. In addition, loss of ZO-1 binding partners Cx40, Cx43, CAR, α-catenin, or vinculin in cardiomyocytes all disrupt heart function[23, 25–29] and loss of CAR results in decreased ZO-1 localization at the intercalated disc[26, 27]. Taken together, these data suggest ZO-1 may be required for intercalated disc structure and function.

Given previous studies suggesting the importance of ZO-1 at the intercalated disc[17, 30], we sought to understand how ZO-1 might affect cardiac physiology. To circumvent the embryonic lethality of constitutive total body ZO-1 knockout[31], we developed inducible heart-specific *Tjp1* deletion mouse models that allow for interrogation of the role for ZO-1 in the adult myocardium and conduction system. We show that ZO-1 is critical to AV nodal conduction and only modestly contributes to ventricular myocardial function. These data shed insight into the role of ZO-1 and potentially other ZO-1 associated proteins in heart physiology.

METHODS

Data availability.

All supporting data and materials presented within this article and in the Data Supplement are available from the corresponding authors by reasonable request. Please see the Major Resources Table in the Data Supplement.

Generation of adult, cardiac specific ZO-1 deficient mice.

All protocols were approved by The University of Chicago Institutional Animal Care and Use Committee. *Tjp1* floxed mice (*Tjp1*$^{tm2c(KOMP)Wtsi}$, MGI:6272009) were generated by Jerrold Turner (The University of Chicago and Brigham and Woman's Hospital) from *Tjp1*$^{tm2a(KOMP)Wtsi}$ (MGI:4451268, KOMP repository, University of California, Davis) mice and generously provided by Jerrold Turner[32]. This was performed by crossing *Tjp1*$^{tm2a(KOMP)Wtsi}$ C57BL/6N mice with B6.Cg-Tg(ACTFLPe)9205Dym/J (MGI: 2448985) mice to delete the En2SA-LacZ-neo cassette between the Frt sites[32]. *Tjp1* floxed mice were bred with mice expressing a tamoxifen inducible Cre recombinase driven by the *Myh6* (B6.FVB(129)-*A1cf*$^{Tg(Myh6-cre/Esr1*)1Jmk/J}$, MGI:3050453)[33], *Hcn4*

(*Hcn4*$^{tm2.1(cre/ERT2)Sev}$, MGI:5529675)[34] , or *Kcne1* (Tg(Kcne1-cre/ERT2)1Imos, MGI:5301931)[35] promoter. To induce recombination, both male and female mice were injected with tamoxifen at 6–8 weeks of age as previously described[36]. *Tjp1*$^{fl/fl}$ littermates with no Cre were also dosed with tamoxifen and used as controls.

Gene expression analysis.

Left ventricular tissue was harvested from anesthetized mice. RNA extraction, reverse transcription, and quantitative real time PCR was performed as previously described[37]. Mouse *Tjp1* expression was measured by quantitative real-time PCR with exon 3 spanning primers specific to the deletion, F: 5'-TTTCAGAGTGGGGAAACCTCC-3', R: 5'-CACTCTTCCTTAGCTGCTGAAC-3'. Transcript abundance was normalized to *Gapdh*.

Western blot analysis.

Following heart harvest, left ventricular and AV node was identified and dissected under a dissecting microscope. These tissues were processed and tissue homogenates were made as previously described[38]. Bradford assay was used to determine the protein concentration of the homogenates and 25 μg of protein was loaded onto 5% (homemade) or 4–20% (Bio-rad) acrylamide gels for separation by SDS-PAGE. Immunoblotting and detection were performed as previously described[38]. Mouse anti-ZO-1 antibody (Thermo Fisher, Waltham, MA, Catalog # 339100) and Rabbit anti-GAPDH (Cell Signaling Technology, Catalog #5174) were used at 1:1000 dilution. CAR (Santa Cruz Biotechnology, Catalog #sc-373791), Cx40 (Thermo Fisher Scientific, Catalog # 37–8900), β-catenin (Cell Signaling Technology, Catalog #9562), and HCN4 (Abcam, Catalog #ab32675) were used at 1:300 dilution. Mouse, Rat, and Rabbit HRP conjugated secondary antibodies were used at 1:1000 dilution (Cell Signaling Technology, Catalog #7076, 7077, 7074 respectively). Blots were developed by enhanced chemiluminescence reagents (Promega, Madison, WI) and imaged using X-ray film or a ChemiDoc XRS system (Bio-rad).

Electrocardiogram recordings.

ECGs were recorded as previously described[37, 39, 40]. Briefly, mice were implanted with subcutaneous telemetry transmitters and recorded over 48 hours (ETA-F10; Data Science International, St. Paul, MN)[39]. Arrhythmia analysis and measurement of ECG intervals were carried out using Ponemah Physiology Platform software (Data Science International, St. Paul, MN).

In vivo electrophysiology.

In vivo electrophysiology was performed as previously described[37]. A right internal jugular venous approach was used on anesthetized mice to make recordings from the atrium, His bundle and ventricle via a Scisense 1.9 F octapolar catheter with 0.5 mm spacing (Transonic, Ithaca, NY) connected to ADI BioAmp and PowerLab apparatus (ADInstruments, Colorado Springs, CO). Data were recorded using LabChart Software (ADInstruments). Atrial and ventricular pacing protocols were driven by a custom Python-based pacing program. Effective refractory periods were measured using 8-beat S1 drive trains followed by a single extra-stimulus.

Echocardiography.

Echocardiography was performed on anesthetized mice as previously described[37]. The heart was imaged with a Vevo 770 ultrasound (VisualSonics, Toronto, Canada) using a 30 MHz high-frequency transducer. B- and M-mode images were recorded in the parasternal long- and short-axis projections at the mid-papillary muscle level in both views. Left ventricular internal diameters, septal wall thickness, and posterior wall thickness were measured in at least three beats from each projection and averaged, and fractional shortening was calculated and used to determine left ventricular ejection fraction.

Ex vivo optical mapping.

Optical mapping was performed as previously described[37] using an approved George Washington University animal protocol. Hearts were isolated and prepared as previously described[41]. Briefly, a midsternal incision was performed on the mice, and hearts were excised and mounted on a Langendorff apparatus for retrograde perfusion and superfusion with warmed (37 °C) and oxygenated (95% O_2/ 5% CO_2) Tyrode's solution (in mM: 128.2 NaCl, 4.7 KCl, 1.05 $MgCl_2$, 1.3 $CaCl_2$, 1.19 NaH_2PO_4, 20 $NaHCO_3$, 11.1 Glucose). Each isolated heart was pinned at the apex to bottom of the chamber to prevent stream-induced movement. After pinning the right atrial and left atrial appendages, the excitation-contraction uncoupler blebbistatin (10 μM, Bio-techne, Minneapolis, MN) was used to eliminate motion artifacts from the optical signals.

Langendorff-perfused hearts were stained in line with perfusion with the voltage-sensitive dye di-4-ANEPPS (30 μl of a 2.6 mM stock solution dissolved in DMSO). Epicardial depolarization was measured by illuminating the tissue preparation with a 520 nm LED light. Emitted light was recorded through a 650 nm long-pass filter by a MiCAM Ultima-L CMOS camera (SciMedia) with high spatial (100 × 100 pixels, 230 ± 20 μm/pixel) and temporal (1000–3000 frames/s) resolution. The acquired fluorescent signal was analyzed with custom-developed software[42].

Immunofluorescence staining.

5 μm thick cryosections of mouse left ventricular tissue or 10 μm AV node containing tissue were fixed (1% PFA), washed (1xPBS), quenched (50 mM NH_4Cl), permeabilized (0.5% NP-40), and stained with primary antibody as previously described[43]. Antibodies were used against the following intercalated disc proteins: ZO-1 (Thermo Fisher Scientific, Catalog # 339100), ZO-2 (Thermo Fisher Scientific, Catalog #71–1400), Cx43 (Cell signaling technology, Catalog # 3512), JUP (Abcam Catalog #ab11799), Nav1.5 (Abcam, Catalog #ab56240), β-catenin (Cell Signaling Technology, Catalog #9562), N-cadherin (Thermo Fisher Scientific, Catalog #333900), CAR (Santa Cruz Biotechnology, Catalog #sc-373791), Cx45 (Thermo Fisher Scientific, Catalog #PA5–77357), Cx40 (Thermo Fisher Scientific, Catalog # 37–8900), and CD31 (Antio-Proteomie, Catalog # mAP-0032). The sections were then stained with Alexa Fluor dye conjugated secondary antibodies (Jackson ImmunoResearch Laboratories, Inc, Catalog #s 711-586-152,715-546-151), phalloidin (Thermo Fisher Scientific, Catalog# A22287), and Hoechst 33342 (Thermo Fisher Scientific, Catalog# 953557). ProLong Gold (Thermo Fisher Scientific, Catalog# P36934) was used for mounting. Fluorescence images were taken using an IX81 Olympus

microscope (Olympus, Waltham, MA) with 20x or 40x air or oil immersion objectives. Quantification was performed in MetaMorph 7 Image Analysis Software (Molecular Devices, San Jose, CA) with linescan of the fluorescence signal across the width of the intercalated disc. Control experiments using the appropriate secondary antibody alone was performed simultaneously with all immunofluorescence staining experiments to determine antibody specificity. Further, for ZO-1, CAR, β-catenin, and JUP, gastrointestinal tissue was used as a positive control for the antibody. Blinded imaging and quantification were performed using identical exposures and matched imaging and processing conditions.

Immunohistochemistry.

Immunohistochemical staining for ZO-1 was performed using anti-ZO-1 (Thermo Scientific, Cat#339100, mouse monoclonal antibody, Clone: ZO-1–1A12,) on formalin fixed paraffin embedded mouse heart sections. After deparaffinization and rehydration, tissue sections were treated with antigen retrieval solution (Agilent, Santa Clara, CA) in a steamer for 20 minutes. MOM blocking kit (Vector Laboratories, Burlingame, CA) was used. Anti-ZO-1 antibody (1:50) was applied on tissue sections for one hour incubation at room temperature in a humidity chamber. Following PBS wash, the antigen-antibody binding was detected with Envision+ system (Agilent) and DAB+ chromogen (Agilent). Tissue sections were counterstained with hematoxylin and mounted. Hematoxylin and eosin stain[44] and trichrome stain (Millipore-Sigma, St. Louis, MO) were performed using standard protocols. Slides were imaged using a Leica DM2000 Microscope (Leica Microsystems, Wetzlar, Germany) with a ProgRes C14^{plus} color digital camera (Jenoptik, Jena, Germany). Control slides using the appropriate secondary antibody alone was used to confirm primary antibody specificity.

Use of human atrial tissue.

Human heart tissue was collected from organ donors (that were not used for heart transplantation, but had no history of major cardiovascular diseases and had normal cardiac function) provided by Illinois Gift of Hope Organ & Tissue Donor Network (GOH). The studies were approved by the Human Study Committee of Rush University. The AV node containing region was dissected out and fixed with formalin. Immunofluorescence and IHC staining of AV node slides were performed using anti ZO-1 (described above) and anti-Cx40 (Thermo Fisher Scientific, Catalog # 37–8900) antibodies with the secondary antibodies described above. Immunofluorescence images were obtained using an Olympus IX81 Inverted Widefield Microscope (Olympus, Waltham, MA).

Transmission electron microscopy.

AV node and surrounding tissues were dissected from mice two weeks post tamoxifen treatment. Tissues were fixed, embedded, sectioned and mounted onto carbon grids as previously described with the following differences[45]. For primary fixation, 2% glutaraldehyde and 4% paraformaldehyde in 0.1M sodium cacodylate buffer was used. 1% osmium tetroxide was used for secondary fixation. Polymerization was done at 60 °C for 48 hours in a vacuum oven. 60 nm thickness sections were cut and mounted on carbon-coated copper grids. Brief staining in 100% uranyl acetate and lead citrate was performed. Semi-thin sections used for Toluidine blue staining were cut at 300 nm. Images were taken with a JEM-1400 Plus electron microscope (JEOL, Tokyo, Japan).

Statistics.

Data are reported as mean ± standard error of the mean (SEM). For paired comparisons, Shapiro-Wilk tests were performed, in R studio (Boston, MA), to determine normality, followed by two-tailed Student's t-tests, in Excel (Microsoft, Redmond, WA), unless otherwise noted. To confirm statistical significance derived from t-tests, non parametric Wilcoxon rank sum test was used and significance is stated when sample sizes were low and normality could not be reliably determined. This is designated with "WRS" followed by the p-value. For count-based quantification of heart-block occurrence, one-tailed Fisher's exact test was performed by using R studio. In the cases that multiple parameters are obtained and compared in the same experiement, the number of tests are limited, and the experiments and analyses are performed sequentially rather than simultaneously. In addition, different types of assays were performed to support our conclusions. While we deem it appropriate to not perform multiple testing correction in the results shown here, we do report the confidence interval and acknowledge that the interpretation could potentially be considered a weakness of our study. Statistical significance is designated as *p<0.05, **p<0.01, and ***p<0.001 in the figures.

RESULTS

Generation of adult cardiac-specific Tjp1 knockout mice.

ZO-1 is widely expressed in multiple cell types and is a known regulator of paracellular permeability in epithelial and endothelial cells[1–4, 12, 13]. Although ZO-1 localization at the intercalated disc is well-documented[16–18, 46, 47], the function of ZO-1 in the heart remains poorly defined. Since complete loss of ZO-1 is embryonic lethal at day E11.5 due to vascular defects[31], we generated inducible tissue-specific knockout models to study cardiac-specific ZO-1 function. *Tjp1* floxed mice were bred with cardiomyocyte-specific (Myh6 promoter) Cre/Esr1* transgenic mice (Fig. 1A)[32, 33].

We first assessed *Tjp1* deletion efficiency in the heart. qRT-PCR showed $Tjp1^{fl/fl};Myh6^{Cre/Esr1*}$ heart tissue have decreased *Tjp1* exon3 containing mRNA (46 ± 4% decrease, p=0.0041, WRS: p=0.016) relative to $Tjp1^{fl/fl}$ controls two weeks post-tamoxifen injection (Fig. 1B). In contrast, liver expression of *Tjp1* mRNA was unchanged between $Tjp1^{fl/fl};Myh6^{Cre/Esr1*}$ and $Tjp1^{fl/fl}$ mice (p=0.15). In the left ventricle, ZO-1 protein was reduced by 69 ± 10% (p=0.013, WRS: p=0.029) by western blot (Fig. 1C). The partial loss of *Tjp1* mRNA and ZO-1 protein in the left ventricle could be due to 1) incomplete *Tjp1* locus recombination resulting in incomplete knockout or 2) the presence of non-cardiomyocyte cells (such as endothelial cells and fibroblasts) not affected by cardiomyocyte specific MerCreMer protein activity. To differentiate between these two possibilities, we next performed immunofluorescence staining for ZO-1 protein to determine its myocardial-specific expression. ZO-1 expression remained abundant in endothelial cells, as identified by CD31 (Fig. 1D arrowheads). ZO-1 protein expression at the intercalated discs was significantly reduced (73 ± 8% decrease, p=0.019, WRS: p=0.050) (Fig. 1D,E arrows, F) as measured by peak intensity of immunofluorescence staining of ZO-1 at the intercalated disc. These findings support that incomplete *Tjp1* knockout is due to a combination of both

factors discussed above. There were no observed differences in cardiomyocyte actin organization or cell morphology.

Loss of ZO-1 disrupts cardiac conduction.

To study the physiologic role of ZO-1 in the heart, we first monitored mice longitudinally by electrocardiogram (ECG) under anesthesia. Five d after tamoxifen treatment, *Tjp1*$^{fl/fl}$*; Myh6*$^{Cre/Esr1*}$ mice had significantly prolonged PR interval (80 ± 10% prolongation, p=4.8e-4) (Fig. 2A, B), indicating 1st degree AV block. By 10 d post-tamoxifen, 4 of 11 mice (p=0.037, one- tailed Fisher's exact test was used because the fraction of mice with AV block can only increase from control) displayed complete dissociation of atrial and ventricular depolarization, indicating heart block with junctional escape rhythm, compared to none (0 of 12) in control mice (Fig. 2C). Ambulatory telemetric electrocardiogram recordings were performed to assess RR and PR interval variation. At one week post-tamoxifen injection, Poincaré plots of the PR interval showed distinct separation between *Tjp1*$^{fl/fl}$*; Myh6*$^{Cre/Esr1*}$ and *Tjp1*$^{fl/fl}$ control mice (Fig. 2D) and average PR interval was significantly prolonged in *Tjp1*$^{fl/fl}$*; Myh6*$^{Cre/Esr1*}$ mice (p=0.00021, WRS: p=0.050) (Fig. 2E). In contrast, dispersion of RR interval and average RR interval were not significantly different (p=0.98). (Fig. 2F,G). By two weeks post-tamoxifen injection, PR interval was not only prolonged, but also highly variable, consistent with 3rd degree heart block and/or junctional escape rhythm (p=0.020, WRS: p=0.050). RR intervals remained not significantly different (p=0.21) (Fig. 2H–K). Neither P wave (10.2 ± 0.8 ms *vs.* 12.3 ± 0.7 ms, p=0.18) nor QRS complex durations (8.9 ± 0.4 ms *vs.* 10.4 ± 0.5 ms, p=0.13) were altered between *Tjp1*$^{fl/fl}$ and *Tjp1*$^{fl/fl}$*; Myh6*$^{Cre/Esr1*}$ mice. Additionally, tamoxifen-injected *Myh6*$^{Cre/Esr1*}$ control mice exhibited normal PR interval lengths (PR=32.7 ± 14 ms). To confirm the specific location of the conduction defect, intracardiac electrophysiology studies were performed. Ten d after tamoxifen injection, the time interval from atrial to bundle of His depolarization was increased (A-H Interval, p=0.0027, WRS: p=0.050, Fig. 2L, M), but the interval from bundle of His depolarization to ventricular depolarization was unchanged (H-V Interval, p=0.39, Fig. 2L, N). The minimum cycle duration that is capable of maintaining 1:1 atrial to ventricular conduction time (Fig. 2O; AV Wenckebach time) was prolonged (p=0.041, WRS:p=0.032). Together, A-H interval and AV Wenckebach prolongation are indicative of slowed AV nodal conduction. Intracardiac pacing studies showed normal atrial and ventricular refractory periods (AERP p=0.50, VERP p=0.25, not shown). These data suggest that removal of ZO-1 causes slowed AV nodal conduction, but does not alter atrial myocardial conduction, ventricular myocardial conduction, or RR interval.

To assess epicardial depolarization patterns, we performed optical mapping studies. Propagation of epicardial depolarization in isolated hearts from mice 20 d post-tamoxifen treatment was measured. The overall pattern of atrial and ventricular depolarization was not different between *Tjp1*$^{fl/fl}$ and *Tjp1*$^{fl/fl}$*; Myh6*$^{Cre/Esr1*}$ hearts with only one focus of depolarization initiation occurring at or near the sinoatrial node in both genotypes (Fig. 3A). There were no significant differences observed in atrial (p=0.86) and ventricular (p=0.84) activation times (Fig. 3A, B). However, a 75 ± 24% increase in AV conduction time was observed (p=0.0045, WRS: p=0.0043), consistent with electrophysiology studies (Fig. 3 and Fig. 2A, B, L, M, O).

Tjp1 deletion is associated with modestly decreased heart function.

Given the observed changes in conduction, we next asked whether loss of cardiomyocyte *Tjp1* would cause decreased heart function. We measured left ventricular ejection fraction by echocardiography over the course of 10 weeks. Ejection fraction was unchanged in $Tjp1^{fl/fl}; Myh6^{Cre/Esr1*}$ compared to $Tjp1^{fl/fl}$ controls in the first 10 d post-tamoxifen (p=0.15). Beginning at 20 d post-tamoxifen treatment, average ejection fraction in $Tjp1^{fl/fl}; Myh6^{Cre/Esr1*}$ mice was slightly decreased compared to $Tjp1^{fl/fl}$ controls (16 ± 4%, p=5.3e-5). (Online Figure IA, B). 40 d post-tamoxifen injection, the decreased ejection fraction in $Tjp1^{fl/fl}; Myh6^{Cre/Esr1*}$ mice persisted without additional decrease in ejection fraction (Online Figure IB). A repeated measures mixed ANOVA was performed and ejection fraction between $Tjp1^{fl/fl}$ and $Tjp1^{fl/fl}; Myh6^{Cre/Esr1*}$ mice was significantly different (p=5.1e-4 and partial eta squared=0.95). The heart rate was not significantly different at any time point (Online Figure IB). Left ventricular systolic and diastolic diameters are shown in Online Figure IIA–F. The small and persistent decrease in ejection fraction in $Tjp1^{fl/fl}; Myh6^{Cre/Esr1*}$ mice at ≥20 d is due predominantly to increased internal diameter (p=0.0017, Online Figure IIC) during systole without significant reduction in diastolic diameter (p=0.090, Online Figure IID). The change in ejection fraction was not accompanied by gross or microscopic changes, including heart size (Online Figure IC), heart weight (Online Figure ID), or fibrosis as determined by trichrome staining (Online Figure IE) 12 weeks after tamoxifen injection. Thus, loss of ZO-1 causes only a small but significant change in cardiac function without evidence of gross or histological alterations.

ZO-1 loss disrupts AV nodal Cx40 and CAR localization and perinodal Cx43 localization.

Due to AV nodal dysfunction following *Tjp1* deletion, we assessed AV node morphology and ZO-1 expression in $Tjp1^{fl/fl}$ and $Tjp1^{fl/fl}; Myh6^{Cre/Esr1*}$ mice. Using trichrome staining, we identified the AV node, which was not organizationally disrupted in $Tjp1^{fl/fl}; Myh6^{Cre/Esr1*}$ mice (Fig. 4A). In $Tjp1^{fl/fl}$ mice, immunohistochemical staining showed ZO-1 was highly expressed at the AV node. ZO-1 staining intensity was decreased by 49 ± 10% (p=0.015, WRS: p=0.050, n=3 for each group) in AV nodes in $Tjp1^{fl/fl}; Myh6^{Cre/Esr1*}$ mice (Fig. 4B). Next, we assessed expression and localization of proteins important to AV nodal conduction. HCN4 staining was high in the region identified as the AV node via trichrome stain (Fig. 4C,D), further confirming its functional specialization. Cx40 and CAR stained the AV node strongly, whereas Cx43 was absent from the AV node, but was strongly expressed in the adjacent myocardium (perinodal region) (Fig 4E,F). Cx40 and CAR co-staining with the intercalated disc marker β-catenin showed that Cx40 and CAR are enriched at intercalated discs of AV nodes (Online Figure III). Cx40 staining intensity within the intercalated discs of the AV node was decreased by 70 ± 8% in $Tjp1^{fl/fl}; Myh6^{Cre/Esr1*}$ mice (p=0.050, WRS: p=0.050, n=3 animals per genotype) (Fig. 4G). Cx43 staining intensity at the intercalated discs of perinodal myocardium was decreased by 65 ± 4% in $Tjp1^{fl/fl}; Myh6^{Cre/Esr1*}$ mice (p=0.0018, WRS: p=0.050, n=3 animals per genotype) (Fig. 4H). CAR stained AV nodal cells in a punctate and membranous pattern at cell-to-cell junctions, and staining intensity was decreased by 39 ± 6% in $Tjp1^{fl/fl}; Myh6^{Cre/Esr1*}$ mice (p=0.011, WRS: p=0.050, n=3 animals per genotype) (Fig. 4I). Cx45, $Na_V1.5$, β-catenin and N-cadherin staining intensity were not changed in the AV node (Online Figure IV).

To determine whether overall Cx40 and CAR protein abundance is altered, we performed western blot for ZO-1, Cx40, and CAR using homogenates of dissected AV nodes. AV nodal tissue dissection was confirmed by enrichment of HCN4 in AV nodal tissue relative to ventricular tissue (Fig. 4J). We observed that ZO-1 and Cx40 protein abundance was decreased by 50 ± 6% (p=.0089, WRS: p=0.014) and 59 ± 11% (p=.036, WRS: p=0.029) respectively in dissected AV nodal regions of *Tjp1*$^{fl/fl}$*; Myh6*$^{Cre/Esr1*}$ mice at 2 weeks of age (Fig. 4K,L). CAR protein abundance also showed a downward trend, but it did not reach statistical significance, (p=0.21, Fig. 4K,L). Similar to immunofluorescence staining results, β-catenin protein abundance was not significantly different (p=0.11, Fig. 4K,L). We further tested if similar changes could also occur in ventricular myocardium distant from the AV node. At the ventricular intercalated disc, Cx43 and CAR localization was significantly decreased (p=0.042 and p=0.0032 respectively, WRS: p=0.050 for both, n=3 animals per genotype), but β-catenin distribution was not significantly altered (p=0.21), as assessed by immunofluorescence staining (Online Figure V).

We next examined whether changes in AV node protein localization and total expression would yield discernable AV node ultrastructural changes. Transmission electron microscopy (TEM) was performed on AV node containing sections, as determined by Toluidine blue staining (Online Figure VI A,B). No discernable differences in overall AV node architecture or in the appearance of the intercalated disc were noted between *Tjp1*$^{fl/fl}$*; Myh6*$^{Cre/Esr1*}$ and control mice 2 weeks post-tamoxifen injection (Online Figure VI C,D).

ZO-1 and Cx40 colocalize in human AV nodes.

Similar to our observation of high ZO-1 abundance in mouse AV nodes, we found ZO-1 is also highly expressed in AV nodes of humans (Fig. 5A,B). It is also expressed at intercalated discs of atrial and ventricular cardiomyocytes (Fig. 5A,B). Since Cx40 is a major AV node connexin[48, 49], and Cx40 is decreased in *Tjp1*$^{fl/fl}$*; Myh6*$^{Cre/Esr1*}$, we stained for Cx40 in human AV node samples. ZO-1 colocalizes with Cx40 in both the AV node and atrial myocardial tissue but is not found in the ventricle (Fig. 5C). Taken together, our human and mouse studies suggest abundant ZO-1 expression in the AV node.

Conduction system-specific ZO-1 loss is sufficient to drive heart block.

Upon determining that ZO-1 is abundantly expressed in mouse and human AV nodal tissues, we next tested the contribution of ZO-1 to cardiac conduction specifically by genetic dissection. We generated conduction system specific (*Tjp1*$^{fl/fl}$*; Hcn4*^{CreERt2}) and AV bundle-His-Purkinje specific (*Tjp1*$^{fl/fl}$*; Kcne1*^{CreERt2}) *Tjp1* deletion mouse models. *Tjp1*$^{fl/fl}$*; Hcn4*^{CreERt2} mice developed increased PR interval (148 ± 7% increase, p=2.7e-7, WRS: p=0.029) and dissociation of atrial and ventricular depolarization 2 weeks after the start of tamoxifen treatment (Fig. 6A–C). In contrast, none of the *Tjp1*$^{fl/fl}$*; Kcne1*^{CreERt2} mice demonstrated heart block (Fig. 6A–C). In line with this finding, the abundant ZO-1 expression found in the AV node was not observed in the AV bundle (Online Figure VII). Furthermore, despite the conduction system defects in the *Tjp1*$^{fl/fl}$*; Hcn4*^{CreERt2} mice, there was no evidence of depressed myocardial function (p=0.51, Fig. 7D), in contrast to our observations in *Tjp1*$^{fl/fl}$*; Myh6*$^{Cre/Esr1*}$ mice (Online Figure I A, B). These results show that ZO-1 expression in the conduction system proximal to the His bundle is critical to

conduction. Furthermore, the data suggest myocardial dysfunction is independent of the conduction system defects in cardiac specific *Tjp1* deleted mice.

DISCUSSION

Healthy cardiac conduction and function relies on the coordinated electrical activity of distinct populations of cardiomyocytes. Electrical activity initiated at the SA node must propagate through atrial myocardium, the AV node, His-Purkinje system, and into ventricular myocardium. Disruption of cell-cell conduction results in cardiac arrhythmias and cardiomyopathies, a leading cause of morbidity and mortality worldwide[50–53]. Intercalated disc proteins have been recognized as important regulators of cardiac conduction due to their function in maintaining electrical and physical coupling between cells. Here we show inducible loss of the intercalated disc protein ZO-1 in cardiomyocytes of adult mice impedes AV node conduction and modestly affects ejection fraction.

Mice with induced cardiomyocyte specific *Tjp1* deletion (*Tjp1*$^{fl/fl}$; *Myh6*$^{Cre/Esr1*}$ mice with tamoxifen injection) exhibit an AV nodal conduction defect with normal atrial and ventricular conduction (Figs. 2,3). This interpretation is based on electrophysiological and optical mapping studies demonstrating increased PR interval, increased AH intervals, increased AV Wenckebach time, and AV conduction time but unchanged HV interval, P wave, QRS complex duration, and atrial and ventricular activation time in *Tjp1*$^{fl/fl}$; *Myh6*$^{Cre/Esr1*}$ mice (Figs. 2,3). To assess 1) if the AV block is intrinsic to the conduction system or secondary to myocardial changes, and 2) to assess potential region-specific requirements of ZO-1 in the conduction system, we generated two additional inducible tissue-specific knockout models. Similar to induced cardiomyocyte specific *Tjp1* knockout (*Tjp1*$^{fl/fl}$; *Myh6*$^{Cre/Esr1*}$), tamoxifen-induced overall conduction system *Tjp1* knockout (*Tjp1*$^{fl/fl}$; *Hcn4*^{CreERt2}) resulted in AV block without decreased ejection fraction (Fig. 6), suggesting AV block is not secondary to myocardial changes. In contrast, tamoxifen-induced *Tjp1* knockout distal to the AV node (*Tjp1*$^{fl/fl}$; *Kcne1*^{CreERt2}) did not manifest heart block. Taken together with our observation that ZO-1 is highly expressed in the AV node, but in the fast conducting AV-bundle, such high expression was not apparent (Online Figure VII), these results support that ZO-1 loss in the conduction system above the bundle of His is responsible for PR prolongation and ZO-1 expression is critical to normal AV nodal conduction.

Given the observed AV node dysfunction following ZO-1 loss, we hypothesized that ZO-1 is important to the organization of proteins at the intercalated disc that facilitate cell-cell conduction. Immunofluorescence microscopy and western blot studies showed decreased expression of Cx40[49, 54] and to a lesser extent, CAR[26, 27], in the AV node in *Tjp1*$^{fl/fl}$; *Myh6*$^{Cre/Esr1}$ mice. This is in line with previous biochemical data demonstrating that connexins, CAR, and ZO-1 can reside within the same protein complex. Connexins contain a C-terminal PDZ binding sequence that directly binds to the PDZ domains of ZO-1[16, 22, 55–57]. CAR contains a PDZ binding C-terminal motif and can precipitate with ZO-1[19, 26, 58, 59]. Furthermore, genetic deletion of *Gja5* (Cx40)[49, 54] and *Cxadr* (CAR)[26, 27] both slow AV nodal conduction. Together these data suggest ZO-1 plays a key role in maintaining the connexin-ZO-1-CAR complex at the intercalated disc.

It is notable that although PR interval was altered in cardiac and conduction system specific *Tjp1* deleted mice, there was no change in RR interval or heart rate. This observation of AV block with normal heart rate is in contrast to some models in which PR interval prolongation is associated with increased RR interval[60, 61]. Interestingly, PR prolongation with normal heart rate is also observed in *Cxadr*[26, 27] and *Gja5*[49] knockout mice. Our finding that CAR localization at the intercalated disc is affected by *Tjp1* knockout along with biochemical interactions between ZO-1, CAR, and Cx40 (discussed above) and altered ZO-1 distribution in *Cxadr* knockout mice provide increasing evidence for functional interactions between these proteins. Together, these observations coalesce into a model in which ZO-1, CAR, and Cx40 physically associate to co-regulate AV nodal conduction.

Although atrial and ventricular conduction speed were normal in $Tjp1^{fl/fl}; Myh6^{Cre/Esr1}$ mice, changes in ventricular intercalated disc organization and protein staining were still observed. By immunofluorescence microscopy, there was decreased Cx43 and CAR localization at the ventricular intercalated disc. These observations are consistent with previous findings that partial connexin loss is not sufficient to induce altered myocardial conduction[62, 63, 64], and *Cxadr* (CAR) deletion in cardiomyocytes also does not significantly affect atrial and ventricular conduction, despite decreased connexin and ZO-1 localization at intercalated discs of ventricular cardiomyocytes[26, 27]. Our finding that *Tjp1* knockout mice have prolonged AV nodal conduction times but normal ventricular conduction times suggests that AV nodal and ventricular cardiomyocyte conduction have different molecular requirements. Our observations support that AV nodal conduction may be particularly vulnerable to defects in the connexin-ZO-1-CAR complex (Fig. 7).

We demonstrate that ZO-1 loss in myocardial tissue is associated with modestly decreased ejection fraction. In contrast, neither of the conduction specific knockout models demonstrated this phenotype (Fig. 6D). This suggests that loss of ZO-1 can independently affect conduction and ejection fraction, and decreased functional output is due directly to loss of ZO-1 in the myocardium and not secondary to conduction defects. We did not observe a progressive loss of ejection fraction and sudden death of the $Tjp1^{fl/fl}; Myh6^{Cre/Esr1*}$ mice, which could be explained by the presence of compensatory mechanisms that may be important for preserving myocardial function following loss of ZO-1. For example, ZO-2, a closely related protein to ZO-1, may play a role in such compensatory mechanisms. ZO-1 and ZO-2 both work to regulate epithelial function, including tight junction function and apical membrane organization[65–67]. Although we could readily detect ZO-2 expression in cardiac endothelial cells, we failed to detect ZO-2 at the intercalated disc 10 d following ZO-1 knockout (Online Figure VII), long term studies are needed to understand whether ZO-2 along with other protein expression and localization are altered and limit ZO-1 induced myocardial changes.

Recently, *TJP1* variations have been associated with arrhythmogenic cardiomyopathy in patients[68], but AV nodal dysfunction was not observed in the 4 probands studied by Bartoli *et al*[68]. We do not currently know why such a difference exists, and further investigation will be required to determine the potential role of ZO-1 on AV nodal function in humans with arrhythmogenic cardiomyopathy. Another difference between our ZO-1 knockout mouse model and the patients of Bartoli et al[68] is the absence of fibro fatty replacement of

myocardial tissue up to 12 weeks after *Tjp1* deletion in the mice. This difference may be due to the adult onset, cardiomyocyte specific nature of the ZO-1 loss in our mouse model compared to patients carrying pathogenic *TJP1* variants, who have altered ZO-1 function in all cell types, throughout their life. Since ZO-1 may influence many aspects of cardiac (e.g. coronary vasculature) as well as other organ system development and physiological function, the clinical symptoms may be influenced by all of these cell types and organs. Long-term studies will be required to further evaluate whether histological features of arrhythmogenic cardiomyopathy can manifest in mice following knockout of *Tjp1*.

ZO-1 has been implicated in other forms of cardiomyopathy without *Tjp1* mutations. For example, expression of a pathogenic mutant of transmembrane protein 43 (TMEM43) associated with arrhythmogenic cardiomyopathy causes loss of ZO-1 at the intercalated disc-like cell-cell junctions, and decreases cell-cell conduction velocity in HL-1 cells[54]. Furthermore, our analysis of published Gene Expression Omnibus datasets suggest *TJP1* expression is altered in hearts of cardiomyopathy patients (GDS2205 and GDS1362), and isoproterenol treated mice (GDS3684). Together, these findings suggest ZO-1 expression or localization change can influence cardiomyopathy pathogenesis.

In conclusion, we demonstrate ZO-1 is necessary for maintaining gap junction protein expression and localization, and loss of ZO-1 results in AV node dysfunction, and when deleted from myocytes throughout the heart, results in modest decrease in cardiac function. Understanding how ZO-1 function is altered in patients with cardiomyopathy and other heart diseases will be important and may provide novel therapeutic approaches.

Supplementary Material

Refer to Web version on PubMed Central for supplementary material.

ACKNOWLEDGEMENTS

We thank Terri Li, Can Gong, Xin Jiang, and Mark Lingen from The University of Chicago Human Tissue Research Center Core, Yimei Chen, Anthony Chang, and James Brainer for assistance with electron microscopy, and Rostislav Bychkov and Richard Telljohann for assistance with mouse AV node identification. *Tjp1* floxed (*Tjp1*$^{tm2c(KOMP)Wtsi}$) mice were generated and generously provided by Jerrold R. Turner with the support of NIH (R01 DK061931 and R01 DK068271). We thank Sylvia M. Evans for the *Hcn4*^{CreERt2} mice.

SOURCES OF FUNDING

This work was partially supported by NIH grants R01 HL126509, R01 HL114010, and R33 HL123857 (to IM) T32HL007381 and T32GM007281 (to WD).

Nonstandard Abbreviations and Acronyms:

AERP	atrial effective refractory period
AV	atrioventricular
CAR	Coxsackie and adenovirus receptor
CD31	cluster of differentiation 31

Cx	connexin
ECG	electrocardiogram
EM	electron microscopy
GAPDH	glyceraldehyde 3-phosphate dehydrogenase
HCN4	potassium/sodium hyperpolarization-activated cyclic nucleotide-gated channel 4
JUP	junctional plakoglobin
MGI	mouse genome informatics
PDZ	PSD95-DLG1-ZO-1
SA	sinoatrial
TEM	transmission electron microscopy
TJP1	*tight* junction protein 1
TMEM43	transmembrane protein 43
VERP	ventricular effective refractory period
ZO-1	zona occludens 1

REFERENCES

1. Stevenson BR, Siliciano JD, Mooseker MS, Goodenough DA. Identification of zo-1: A high molecular weight polypeptide associated with the tight junction (zonula occludens) in a variety of epithelia. J Cell Biol. 1986;103:755–766 [PubMed: 3528172]
2. Fanning AS, Anderson JM. Zonula occludens-1 and −2 are cytosolic scaffolds that regulate the assembly of cellular junctions. Ann N Y Acad Sci. 2009;1165:113–120 [PubMed: 19538295]
3. Shen L, Weber CR, Raleigh DR, Yu D, Turner JR. Tight junction pore and leak pathways: A dynamic duo. Annu Rev Physiol. 2011;73:283–309 [PubMed: 20936941]
4. Rodgers LS, Beam MT, Anderson JM, Fanning AS. Epithelial barrier assembly requires coordinated activity of multiple domains of the tight junction protein zo-1. J Cell Sci. 2013;126:1565–1575 [PubMed: 23418357]
5. Fanning AS, Jameson BJ, Jesaitis LA, Anderson JM. The tight junction protein zo-1 establishes a link between the transmembrane protein occludin and the actin cytoskeleton. J Biol Chem. 1998;273:29745–29753 [PubMed: 9792688]
6. Itoh M, Furuse M, Morita K, Kubota K, Saitou M, Tsukita S. Direct binding of three tight junction-associated maguks, zo-1, zo-2, and zo-3, with the cooh termini of claudins. J Cell Biol. 1999;147:1351–1363 [PubMed: 10601346]
7. Ebnet K, Schulz CU, Meyer Zu Brickwedde MK, Pendl GG, Vestweber D. Junctional adhesion molecule interacts with the pdz domain-containing proteins af-6 and zo-1. J Biol Chem. 2000;275:27979–27988 [PubMed: 10856295]
8. Furuse M, Itoh M, Hirase T, Nagafuchi A, Yonemura S, Tsukita S. Direct association of occludin with zo-1 and its possible involvement in the localization of occludin at tight junctions. J Cell Biol. 1994;127:1617–1626 [PubMed: 7798316]

9. Maiers JL, Peng X, Fanning AS, DeMali KA. Zo-1 recruitment to α-catenin--a novel mechanism for coupling the assembly of tight junctions to adherens junctions. J Cell Sci. 2013;126:3904–3915 [PubMed: 23813953]
10. Fanning AS, Ma TY, Anderson JM. Isolation and functional characterization of the actin binding region in the tight junction protein zo-1. FASEB J. 2002;16:1835–1837 [PubMed: 12354695]
11. Itoh M, Nagafuchi A, Moroi S, Tsukita S. Involvement of zo-1 in cadherin-based cell adhesion through its direct binding to alpha catenin and actin filaments. J Cell Biol. 1997;138:181–192 [PubMed: 9214391]
12. Tornavaca O, Chia M, Dufton N, Almagro LO, Conway DE, Randi AM, Schwartz MA, Matter K, Balda MS. Zo-1 controls endothelial adherens junctions, cell-cell tension, angiogenesis, and barrier formation. J Cell Biol. 2015;208:821–838 [PubMed: 25753039]
13. Itoh M, Nakadate K, Matsusaka T, Hunziker W, Sugimoto H. Effects of the differential expression of zo-1 and zo-2 on podocyte structure and function. Genes Cells. 2018;23:546–556 [PubMed: 29845705]
14. Roberts JD. Tjp1 mutations in arrhythmogenic cardiomyopathy. Circ Genom Precis Med. 2018;11:e002337 [PubMed: 30354307]
15. Hunter AW, Barker RJ, Zhu C, Gourdie RG. Zonula occludens-1 alters connexin43 gap junction size and organization by influencing channel accretion. Mol Biol Cell. 2005;16:5686–5698 [PubMed: 16195341]
16. Toyofuku T, Yabuki M, Otsu K, Kuzuya T, Hori M, Tada M. Direct association of the gap junction protein connexin-43 with zo-1 in cardiac myocytes. J Biol Chem. 1998;273:12725–12731 [PubMed: 9582296]
17. Vermij SH, Abriel H, van Veen TA. Refining the molecular organization of the cardiac intercalated disc. Cardiovasc Res. 2017;113:259–275 [PubMed: 28069669]
18. Bruce AF, Rothery S, Dupont E, Severs NJ. Gap junction remodelling in human heart failure is associated with increased interaction of connexin43 with zo-1. Cardiovasc Res. 2008;77:757–765 [PubMed: 18056766]
19. Cohen CJ, Shieh JT, Pickles RJ, Okegawa T, Hsieh JT, Bergelson JM. The coxsackievirus and adenovirus receptor is a transmembrane component of the tight junction. Proc Natl Acad Sci U S A. 2001;98:15191–15196 [PubMed: 11734628]
20. Kausalya PJ, Reichert M, Hunziker W. Connexin45 directly binds to zo-1 and localizes to the tight junction region in epithelial mdck cells. FEBS Lett. 2001;505:92–96 [PubMed: 11557048]
21. Flores CE, Li X, Bennett MV, Nagy JI, Pereda AE. Interaction between connexin35 and zonula occludens-1 and its potential role in the regulation of electrical synapses. Proc Natl Acad Sci U S A. 2008;105:12545–12550 [PubMed: 18719117]
22. Li X, Olson C, Lu S, Kamasawa N, Yasumura T, Rash JE, Nagy JI. Neuronal connexin36 association with zonula occludens-1 protein (zo-1) in mouse brain and interaction with the first pdz domain of zo-1. Eur J Neurosci. 2004;19:2132–2146 [PubMed: 15090040]
23. Nagasawa K, Chiba H, Fujita H, Kojima T, Saito T, Endo T, Sawada N. Possible involvement of gap junctions in the barrier function of tight junctions of brain and lung endothelial cells. J Cell Physiol. 2006;208:123–132 [PubMed: 16547974]
24. Zemljic-Harpf AE, Godoy JC, Platoshyn O, Asfaw EK, Busija AR, Domenighetti AA, Ross RS. Vinculin directly binds zonula occludens-1 and is essential for stabilizing connexin-43-containing gap junctions in cardiac myocytes. J Cell Sci. 2014;127:1104–1116 [PubMed: 24413171]
25. Eckardt D, Theis M, Degen J, Ott T, van Rijen HV, Kirchhoff S, Kim JS, de Bakker JM, Willecke K. Functional role of connexin43 gap junction channels in adult mouse heart assessed by inducible gene deletion. J Mol Cell Cardiol. 2004;36:101–110 [PubMed: 14734052]
26. Lim BK, Xiong D, Dorner A, Youn TJ, Yung A, Liu TI, Gu Y, Dalton ND, Wright AT, Evans SM, Chen J, Peterson KL, McCulloch AD, Yajima T, Knowlton KU. Coxsackievirus and adenovirus receptor (car) mediates atrioventricular-node function and connexin 45 localization in the murine heart. J Clin Invest. 2008;118:2758–2770 [PubMed: 18636119]
27. Lisewski U, Shi Y, Wrackmeyer U, Fischer R, Chen C, Schirdewan A, Jüttner R, Rathjen F, Poller W, Radke MH, Gotthardt M. The tight junction protein car regulates cardiac conduction and cell-cell communication. J Exp Med. 2008;205:2369–2379 [PubMed: 18794341]

28. Li J, Goossens S, van Hengel J, Gao E, Cheng L, Tyberghein K, Shang X, De Rycke R, van Roy F, Radice GL. Loss of αt-catenin alters the hybrid adhering junctions in the heart and leads to dilated cardiomyopathy and ventricular arrhythmia following acute ischemia. J Cell Sci. 2012;125:1058–1067 [PubMed: 22421363]
29. Zemljic-Harpf AE, Ponrartana S, Avalos RT, Jordan MC, Roos KP, Dalton ND, Phan VQ, Adamson ED, Ross RS. Heterozygous inactivation of the vinculin gene predisposes to stress-induced cardiomyopathy. Am J Pathol. 2004;165:1033–1044 [PubMed: 15331426]
30. Palatinus JA, O'Quinn MP, Barker RJ, Harris BS, Jourdan J, Gourdie RG. Zo-1 determines adherens and gap junction localization at intercalated disks. Am J Physiol Heart Circ Physiol. 2011;300:H583–594 [PubMed: 21131473]
31. Katsuno T, Umeda K, Matsui T, Hata M, Tamura A, Itoh M, Takeuchi K, Fujimori T, Nabeshima Y, Noda T, Tsukita S. Deficiency of zonula occludens-1 causes embryonic lethal phenotype associated with defected yolk sac angiogenesis and apoptosis of embryonic cells. Mol Biol Cell. 2008;19:2465–2475 [PubMed: 18353970]
32. Odenwald MA, Choi W, Kuo WT, Singh G, Sailer A, Wang Y, Shen L, Fanning AS, Turner JR. The scaffolding protein zo-1 coordinates actomyosin and epithelial apical specializations. J Biol Chem. 2018;293:17317–17335 [PubMed: 30242130]
33. Sohal DS, Nghiem M, Crackower MA, Witt SA, Kimball TR, Tymitz KM, Penninger JM, Molkentin JD. Temporally regulated and tissue-specific gene manipulations in the adult and embryonic heart using a tamoxifen-inducible cre protein. Circ Res. 2001;89:20–25 [PubMed: 11440973]
34. Liang X, Wang G, Lin L, Lowe J, Zhang Q, Bu L, Chen Y, Chen J, Sun Y, Evans SM. Hcn4 dynamically marks the first heart field and conduction system precursors. Circ Res. 2013;113:399–407 [PubMed: 23743334]
35. Arnolds DE, Moskowitz IP. Inducible recombination in the cardiac conduction system of mink: Creert² bac transgenic mice. Genesis. 2011;49:878–884 [PubMed: 21504046]
36. Oka T, Maillet M, Watt AJ, Schwartz RJ, Aronow BJ, Duncan SA, Molkentin JD. Cardiac-specific deletion of gata4 reveals its requirement for hypertrophy, compensation, and myocyte viability. Circulation research. 2006;98:837–845 [PubMed: 16514068]
37. Nadadur RD, Broman MT, Boukens B, Mazurek SR, Yang X, van den Boogaard M, Bekeny J, Gadek M, Ward T, Zhang M, Qiao Y, Martin JF, Seidman CE, Seidman J, Christoffels V, Efimov IR, McNally EM, Weber CR, Moskowitz IP. Pitx2 modulates a tbx5-dependent gene regulatory network to maintain atrial rhythm. Sci Transl Med. 2016;8:354ra115
38. Gemel J, Su Z, Gileles-Hillel A, Khalyfa A, Gozal D, Beyer EC. Intermittent hypoxia causes nox2-dependent remodeling of atrial connexins. BMC Cell Biol. 2017;18:7 [PubMed: 28124622]
39. Arnolds DE, Liu F, Fahrenbach JP, Kim GH, Schillinger KJ, Smemo S, McNally EM, Nobrega MA, Patel VV, Moskowitz IP. Tbx5 drives scn5a expression to regulate cardiac conduction system function. The Journal of clinical investigation. 2012;122:2509–2518 [PubMed: 22728936]
40. Dai W, Laforest B, Tyan L, Shen KM, Nadadur RD, Alvarado FJ, Mazurek SR, Lazarevic S, Gadek M, Wang Y, Li Y, Valdivia HH, Shen L, Broman MT, Moskowitz IP, Weber CR. A calcium transport mechanism for atrial fibrillation in tbx5-mutant mice. Elife. 2019;8
41. Glukhov AV, Flagg TP, Fedorov VV, Efimov IR, Nichols CG. Differential k(atp) channel pharmacology in intact mouse heart. J Mol Cell Cardiol. 2010;48:152–160 [PubMed: 19744493]
42. Laughner JI, Ng FS, Sulkin MS, Arthur RM, Efimov IR. Processing and analysis of cardiac optical mapping data obtained with potentiometric dyes. Am J Physiol Heart Circ Physiol. 2012;303:H753–765 [PubMed: 22821993]
43. Weber CR, Raleigh DR, Su L, Shen L, Sullivan EA, Wang Y, Turner JR. Epithelial myosin light chain kinase activation induces mucosal interleukin-13 expression to alter tight junction ion selectivity. J Biol Chem. 2010;285:12037–12046 [PubMed: 20177070]
44. Cardiff RD, Miller CH, Munn RJ. Manual hematoxylin and eosin staining of mouse tissue sections. Cold Spring Harb Protoc. 2014;2014:655–658 [PubMed: 24890205]
45. Graham L, Orenstein JM. Processing tissue and cells for transmission electron microscopy in diagnostic pathology and research. Nat Protoc. 2007;2:2439–2450 [PubMed: 17947985]

46. Barker RJ, Price RL, Gourdie RG. Increased association of zo-1 with connexin43 during remodeling of cardiac gap junctions. Circ Res. 2002;90:317–324 [PubMed: 11861421]
47. Hervé JC, Bourmeyster N, Sarrouilhe D, Duffy HS. Gap junctional complexes: From partners to functions. Prog Biophys Mol Biol. 2007;94:29–65 [PubMed: 17507078]
48. Temple IP, Inada S, Dobrzynski H, Boyett MR. Connexins and the atrioventricular node. Heart Rhythm. 2013;10:297–304 [PubMed: 23085482]
49. Simon AM, Goodenough DA, Paul DL. Mice lacking connexin40 have cardiac conduction abnormalities characteristic of atrioventricular block and bundle branch block. Curr Biol. 1998;8:295–298 [PubMed: 9501069]
50. Severs NJ, Coppen SR, Dupont E, Yeh HI, Ko YS, Matsushita T. Gap junction alterations in human cardiac disease. Cardiovascular research. 2004;62:368–377 [PubMed: 15094356]
51. Landstrom AP, Dobrev D, Wehrens XHT. Calcium signaling and cardiac arrhythmias. Circulation research. 2017;120:1969–1993 [PubMed: 28596175]
52. van Weerd JH, Christoffels VM. The formation and function of the cardiac conduction system. Development. 2016;143:197–210 [PubMed: 26786210]
53. Arnolds DE, Chu A, McNally EM, Nobrega MA, Moskowitz IP. The emerging genetic landscape underlying cardiac conduction system function. Birth defects research. Part A, Clinical and molecular teratology. 2011;91:578–585 [PubMed: 21538814]
54. Kirchhoff S, Nelles E, Hagendorff A, Krüger O, Traub O, Willecke K. Reduced cardiac conduction velocity and predisposition to arrhythmias in connexin40-deficient mice. Curr Biol. 1998;8:299–302 [PubMed: 9501070]
55. Laing JG, Manley-Markowski RN, Koval M, Civitelli R, Steinberg TH. Connexin45 interacts with zonula occludens-1 and connexin43 in osteoblastic cells. J Biol Chem. 2001;276:23051–23055 [PubMed: 11313345]
56. Nielsen PA, Beahm DL, Giepmans BN, Baruch A, Hall JE, Kumar NM. Molecular cloning, functional expression, and tissue distribution of a novel human gap junction-forming protein, connexin-31.9. Interaction with zona occludens protein-1. J Biol Chem. 2002;277:38272–38283 [PubMed: 12154091]
57. Bouvier D, Kieken F, Kellezi A, Sorgen PL. Structural changes in the carboxyl terminus of the gap junction protein connexin 40 caused by the interaction with c-src and zonula occludens-1. Cell Commun Adhes. 2008;15:107–118 [PubMed: 18649183]
58. Coyne CB, Voelker T, Pichla SL, Bergelson JM. The coxsackievirus and adenovirus receptor interacts with the multi-pdz domain protein-1 (mupp-1) within the tight junction. J Biol Chem. 2004;279:48079–48084 [PubMed: 15364909]
59. Sollerbrant K, Raschperger E, Mirza M, Engstrom U, Philipson L, Ljungdahl PO, Pettersson RF. The coxsackievirus and adenovirus receptor (car) forms a complex with the pdz domain-containing protein ligand-of-numb protein-x (lnx). J Biol Chem. 2003;278:7439–7444 [PubMed: 12468544]
60. Fabritz L, Kirchhof P, Fortmüller L, Auchampach JA, Baba HA, Breithardt G, Neumann J, Boknik P, Schmitz W. Gene dose-dependent atrial arrhythmias, heart block, and brady-cardiomyopathy in mice overexpressing a(3) adenosine receptors. Cardiovasc Res. 2004;62:500–508 [PubMed: 15158142]
61. Baruscotti M, Bucchi A, Viscomi C, Mandelli G, Consalez G, Gnecchi-Rusconi T, Montano N, Casali KR, Micheloni S, Barbuti A, DiFrancesco D. Deep bradycardia and heart block caused by inducible cardiac-specific knockout of the pacemaker channel gene hcn4. Proc Natl Acad Sci U S A. 2011;108:1705–1710 [PubMed: 21220308]
62. Thomas SP, Kucera JP, Bircher-Lehmann L, Rudy Y, Saffitz JE, Kléber AG. Impulse propagation in synthetic strands of neonatal cardiac myocytes with genetically reduced levels of connexin43. Circ Res. 2003;92:1209–1216 [PubMed: 12730095]
63. Morley GE, Vaidya D, Samie FH, Lo C, Delmar M, Jalife J. Characterization of conduction in the ventricles of normal and heterozygous cx43 knockout mice using optical mapping. J Cardiovasc Electrophysiol. 1999;10:1361–1375 [PubMed: 10515561]
64. Akar FG, Spragg DD, Tunin RS, Kass DA, Tomaselli GF. Mechanisms underlying conduction slowing and arrhythmogenesis in nonischemic dilated cardiomyopathy. Circ Res. 2004;95:717–725 [PubMed: 15345654]

65. Van Itallie CM, Fanning AS, Bridges A, Anderson JM. Zo-1 stabilizes the tight junction solute barrier through coupling to the perijunctional cytoskeleton. Mol Biol Cell. 2009;20:3930–3940 [PubMed: 19605556]

66. Fanning AS, Van Itallie CM, Anderson JM. Zonula occludens-1 and −2 regulate apical cell structure and the zonula adherens cytoskeleton in polarized epithelia. Mol Biol Cell. 2012;23:577–590 [PubMed: 22190737]

67. Spadaro D, Tapia R, Jond L, Sudol M, Fanning AS, Citi S. Zo proteins redundantly regulate the transcription factor dbpa/zonab. J Biol Chem. 2014;289:22500–22511 [PubMed: 24986862]

68. De Bortoli M, Postma AV, Poloni G, Calore M, Minervini G, Mazzotti E, Rigato I, Ebert M, Lorenzon A, Vazza G, Cipriani A, Bariani R, Perazzolo Marra M, Husser D, Thiene G, Daliento L, Corrado D, Basso C, Tosatto SCE, Bauce B, van Tintelen JP, Rampazzo A. Whole-exome sequencing identifies pathogenic variants in tjp1 gene associated with arrhythmogenic cardiomyopathy. Circ Genom Precis Med. 2018;11:e002123 [PubMed: 30354300]

NOVELTY AND SIGNIFICANCE

What Is Known?

- The tight junction protein, zonula occludens 1 (ZO-1) maintains and regulates barrier function in epithelia and endothelia.
- ZO-1 is found in the heart at cardiomyocyte junctions, called intercalated discs.
- ZO-1 interacts with proteins that regulate cell-to-cell communications, called connexins, as well as other cell-cell junction components.

What New Information Does This Article Contribute?

- Heart block is a common patient condition whereby the electrical signals slow or are blocked as they flow from atria to ventricle.
- Loss of ZO-1 in cardiomyocytes of adult mice results in heart block.
- Atrioventricular (AV) node conduction, the electrical connection between the atria and ventricle, as opposed to conduction is either chamber, is most sensitive to ZO-1 loss.
- Expression and localization of connexin 40, which is important for AV nodal conduction, are disrupted in ZO-1 deleted AV nodes.

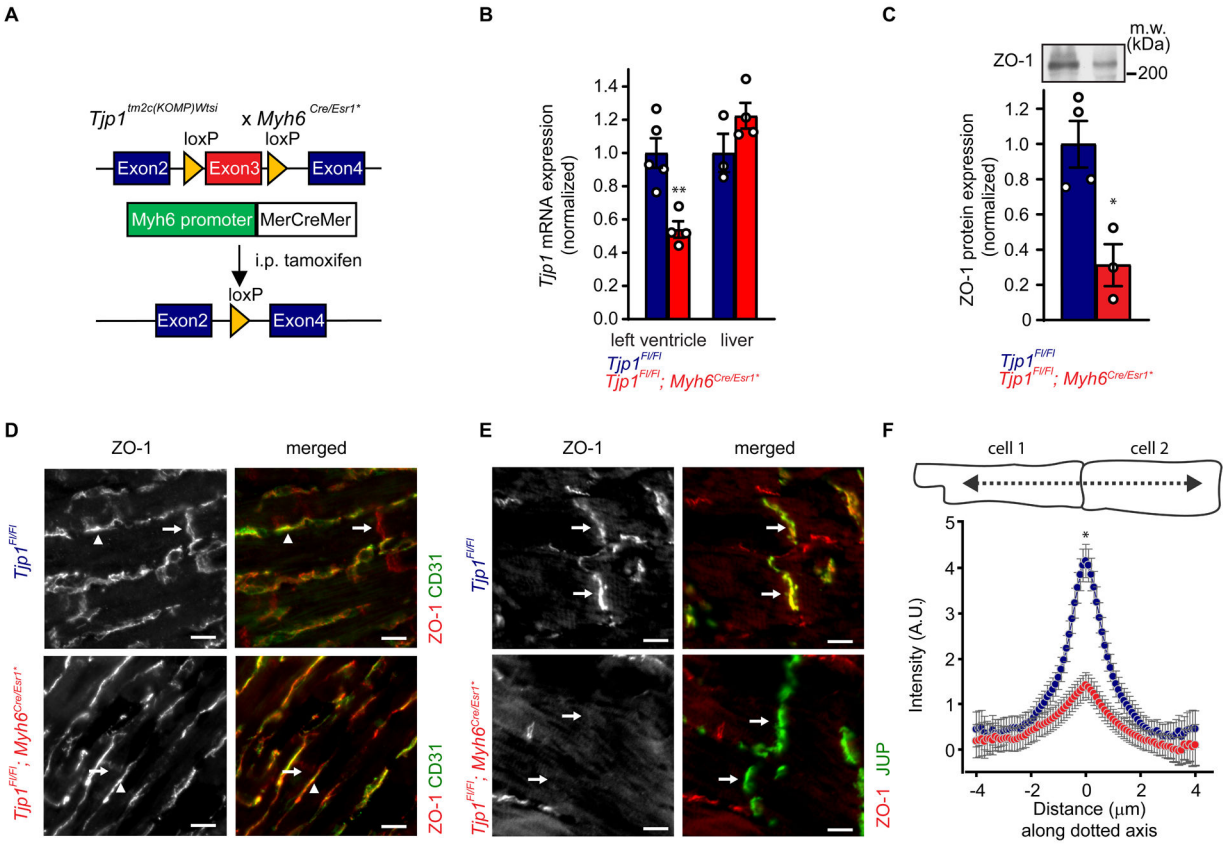

Figure 1: Inducible cardiomyocyte-specific *Tjp1* deletion reduces ZO-1 expression at intercalated discs.

A. Breeding and treatment scheme for *Tjp1* deletion (*Tjp1*$^{fl/fl}$*; Myh6*$^{Cre/Esr1*}$). B. Exon 3 specific *Tjp1* mRNA levels in left ventricle (p=0.0041, WRS: p=0.016, n=5 *Tjp1*$^{fl/fl}$, n=4 *Tjp1*$^{fl/fl}$*; Myh6*$^{Cre/Esr1*}$ mice) and liver (p=0.15, n=3 *Tjp1*$^{fl/fl}$, n=4 *Tjp1*$^{fl/fl}$*; Myh6*$^{Cre/Esr1*}$ mice), as determined by qRT-PCR C. Western blot of left ventricular lysate (p=0.013, WRS: p=0.029, n=4 Tjp1fl$^{/fl}$, n=3 *Tjp1*$^{fl/fl}$*; Myh6*$^{Cre/Esr1*}$ mice). D. Representative images of immunofluorescent staining of ZO-1 in left ventricular tissue. CD31 was used to label endothelial cells. Arrows: intercalated disc, Arrow heads: endothelial cells. E. Representative images of immunofluorescent staining of ZO-1 in left ventricular tissue. Junction plakoglobin (JUP) was co-stained with ZO-1 to mark intercalated discs. Arrow: intercalated disc. F. Immunofluorescent staining along lines perpendicular to the intercalated disc are shown (p=0.019, WRS: p=0.050, n=3 mice per genotype, 18 intercalated discs per animal) (Red: *Tjp1*$^{fl/fl}$*; Myh6*$^{Cre/Esr1*}$, Blue: *Tjp1*$^{fl/fl}$, **p<0.01, * p<0.05). All studies were performed at 10 d post-tamoxifen injection. (Scale bar=10 μm). Two-tailed Student's t-test was used to calculate p-values.

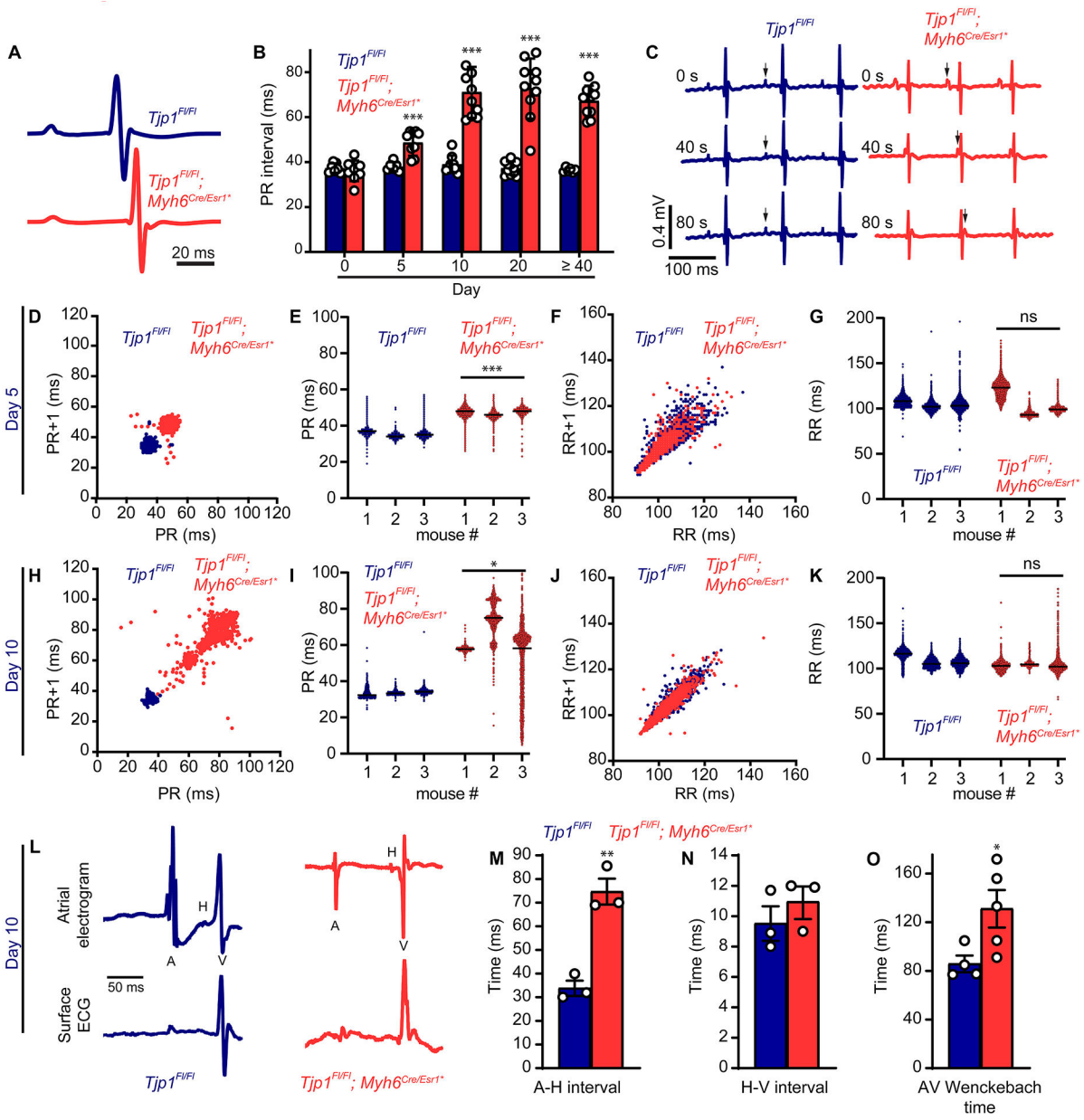

Figure 2: *Tjp1*$^{fl/fl}$*; Myh6*$^{Cre/Esr1*}$ mice have altered cardiac electrophysiology.

A. Averaged telemetry signals 5 d after tamoxifen injection. B. Time course of PR interval following tamoxifen injection (p=0.50 (n=7 *Tjp1*$^{fl/fl}$, n=8 *Tjp1*$^{fl/fl}$*; Myh6*$^{Cre/Esr1*}$) 0 d, p=4.8e-4 (n=6 *Tjp1*$^{fl/fl}$, n=9 *Tjp1*$^{fl/fl}$*; Myh6*$^{Cre/Esr1*}$) for 5 d, p=2.6e-7 (n=9 *Tjp1*$^{fl/fl}$, n=10 *Tjp1*$^{fl/fl}$*; Myh6*$^{Cre/Esr1*}$) for 10 d, p=3.8e-8 (n=11 *Tjp1*$^{fl/fl}$, n=10 *Tjp1*$^{fl/fl}$*; Myh6*$^{Cre/Esr1*}$) for 20 d, and p=3.1e-8 (n=6 *Tjp1*$^{fl/fl}$, n=10 *Tjp1*$^{fl/fl}$*; Myh6*$^{Cre/Esr1*}$) for 40 d or later). C. Sampling of 3 time points within a representative ECG trace in *Tjp1*$^{fl/fl}$ and *Tjp1*$^{fl/fl}$*; Myh6*$^{Cre/Esr1*}$ mice. (arrows: P waves) D, H. Representative Poincaré plots, showing beat-to-beat PR interval variability, from *Tjp1*$^{fl/fl}$*; Myh6*$^{Cre/Esr1*}$ and *Tjp1*$^{fl/fl}$ mice 5 or 10 d post tamoxifen treatment. E, I. PR intervals 5 or 10 d post tamoxifen treatment (p=2.1e-4 for 5 d and p=0.020 for 10d, WRS: p=0.050 for both, based on averages for each mouse. n=3 mice

per genotype). F, J. Representative Poincaré plots, showing beat-to-beat RR interval variability, from *Tjp1*$^{fl/fl}$*; Myh6*$^{Cre/Esr1*}$ and *Tjp1*$^{fl/fl}$ mice 5 or 10 d post tamoxifen treatment. G, K. RR intervals 5 or 10 d post tamoxifen treatment (n=3 mice per genotype). L. Representative atrial electrogram and simultaneous surface ECG recordings (n=animals per genotype). M. Atrial to His conduction time (p=0.0027, WRS: p=0.050, n=3 *Tjp1*$^{fl/fl}$, n=3 *Tjp1*$^{fl/fl}$*; Myh6*$^{Cre/Esr1*}$ mice). N. His to ventricular conduction time (p=0.39, n=3 *Tjp1*$^{fl/fl}$, n=3 *Tjp1*$^{fl/fl}$*; Myh6*$^{Cre/Esr1*}$ mice). O. AV Wenckebach time (p=0.041, WRS: p=0.029, n=4 *Tjp1*$^{fl/fl}$, n=5 *Tjp1*$^{fl/fl}$*; Myh6*$^{Cre/Esr1*}$ mice). (Red: *Tjp1*$^{fl/fl}$*; Myh6*$^{Cre/Esr1*}$, Blue: *Tjp1*$^{fl/fl}$, ***p<0.001, ** p<0.01, *p<0.05, ns indicates not significant) Two-tailed Student's t-test was used to calculate p-values.

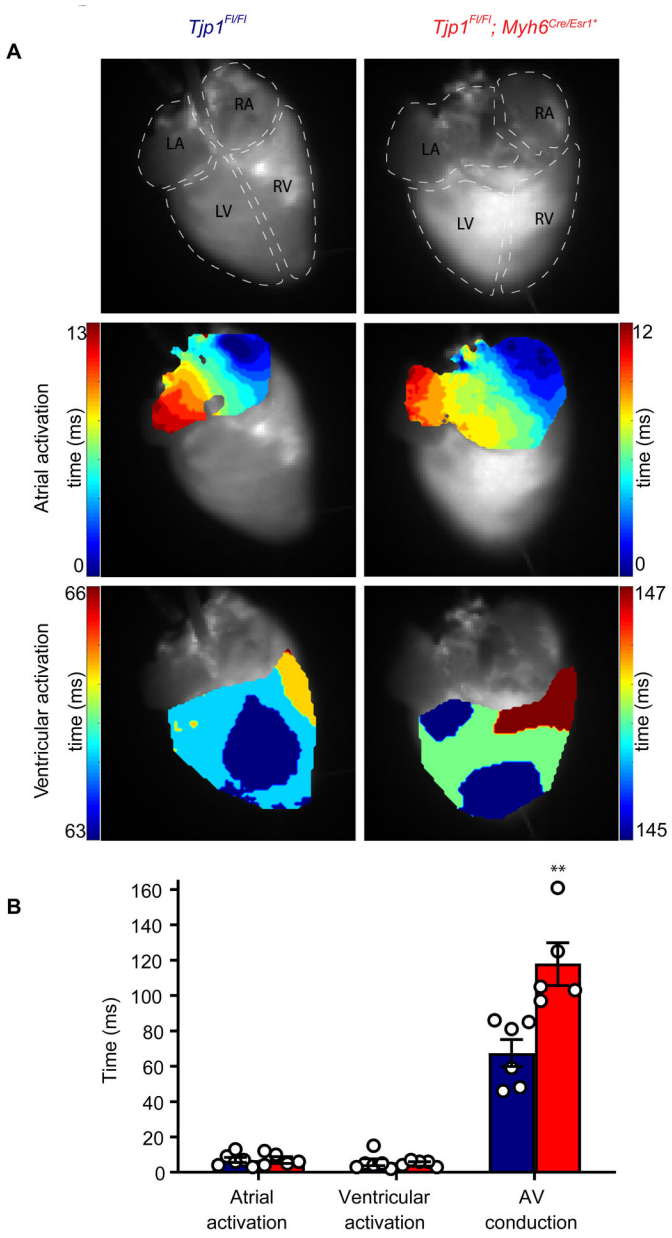

Figure 3: Identification of prolonged AV conduction time by optical mapping.

A. Representative activation maps of atria and ventricle in *Tjp1*$^{fl/fl}$ (left) and *Tjp1*$^{fl/fl}$; *Myh6*$^{Cre/Esr1*}$ (right) mice. B. Atrial, ventricular, AV conduction times (p=0.0045, WRS: p=0.0043, n=6 *Tjp1*$^{fl/fl}$, n=5 *Tjp1*$^{fl/fl}$; *Myh6*$^{Cre/Esr1*}$ mice). All studies were performed 20 d post-tamoxifen injection. (Red: *Tjp1*$^{fl/fl}$; *Myh6*$^{Cre/Esr1*}$, Blue: *Tjp1*$^{fl/fl}$, **p<0.01). Two-tailed Student's t-test was used to calculate p-values.

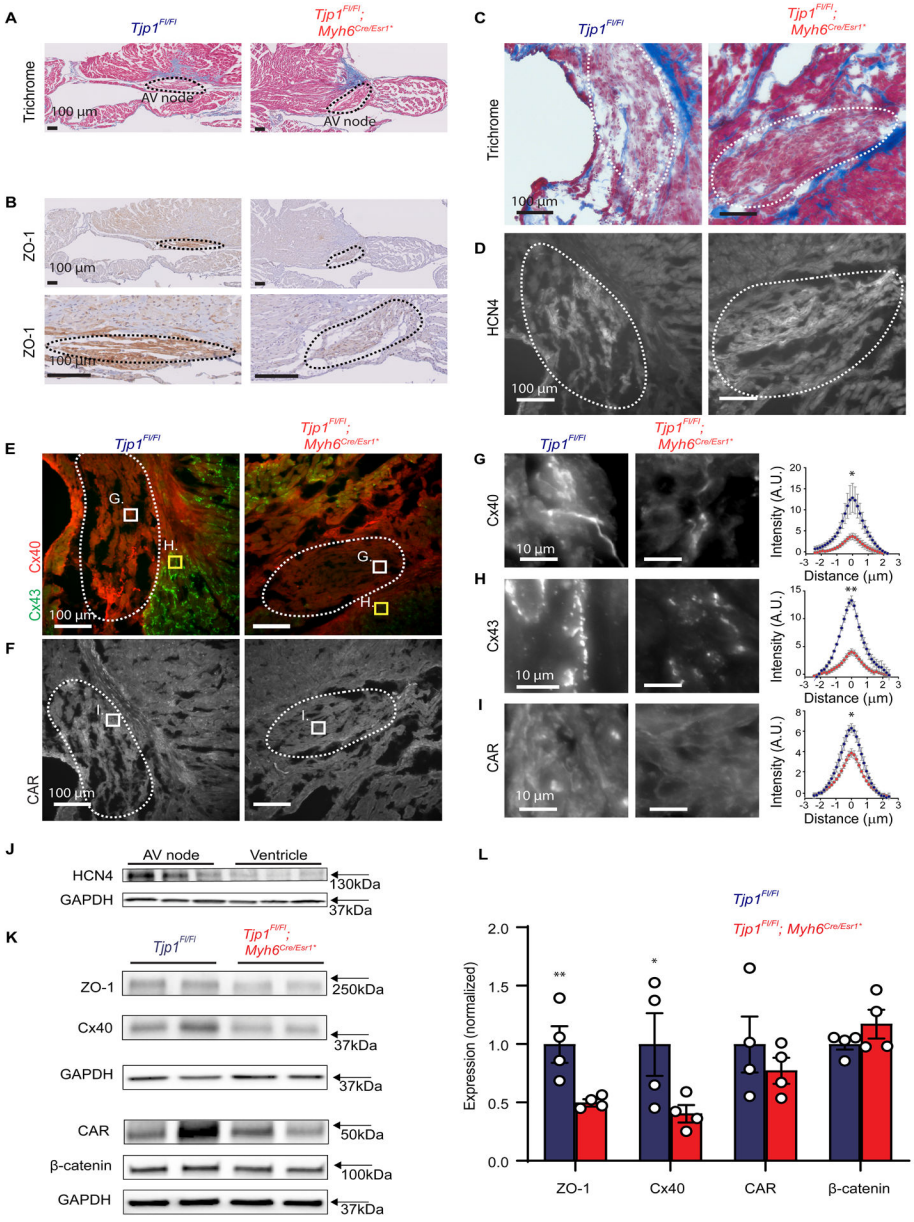

Figure 4: ZO-1 loss disrupts AV node protein localization and abundance.

A. Representative trichrome stain of mouse AV nodes. B. Representative immunohistochemical staining for ZO-1 in AV nodes (Low and high magnification images of the same AV node). C-D. Representative trichrome (C) and HCN4 immunofluorescent (D) staining for AV node identification. E-F. Immunofluorescent staining of Cx40 (E), Cx43 (E), and CAR (F) at low power (scale bar=100 μm). G-I. Representative high power images from boxed region of images in E-F (Cx40 in panel G, within AV node, Cx43 in panel H, in perinodal area, CAR in panel I, within AV node, scale bar=10 μm) and quantification of intercalated disc staining of Cx40 (G, within AV node), Cx43 (G, perinodal area), and CAR (I, within AV node). Quantification of immunofluorescent staining along lines perpendicular to the intercalated disc are shown. Peak intercalated disc intensity values were averaged per

animal and compared (p=0.050 for Cx40, p=0.0018 for Cx43, and p=0.011 for CAR,WRS: p=0.050 for all, n=3 mice per genotype, 8 intercalated disc region measurements per mouse). AV nodes are circled by dashed lines. J. Western blot images of HCN4 expression in AV node tissues compared to ventricular tissue in the same *Tjp1*$^{fl/fl}$ mice (n=3 mice). K. Representative western blot images of AV node ZO-1, Cx40, CAR, and β-catenin and corresponding GAPDH loading control. L. Quantification of western blot (p=0.0089 , WRS: p=0.014 with a 95% confidence interval of 100±24% (*Tjp1*$^{fl/fl}$) and 50±8%(*Tjp1*$^{fl/fl}$; *Myh6*$^{Cre/Esr1*}$) for ZO-1 , p=0.039, WRS: p=0.029 with a 95% confidence interval of 100±42%(*Tjp1*$^{fl/fl}$) and 41±28%(*Tjp1*$^{fl/fl}$; *Myh6*$^{Cre/Esr1*}$) for Cx40, n=4 mice per genotype) (Red: *Tjp1*$^{fl/fl}$; *Myh6*$^{Cre/Esr1*}$, Blue: *Tjp1*$^{fl/fl}$, ***p<0.001, ** p<0.01, *p<0.05. All studies were performed 10 d post-tamoxifen injection. Peak intercalated disc intensity two-tailed Student's t-test was used to calculate p-values from immunofluorescence experiments and one-tailed Student's t-test was used to test our hypothesis in the western blots that ZO-1 and Cx40 were decreased in *Tjp1*$^{fl/fl}$; *Myh6*$^{Cre/Esr1*}$.

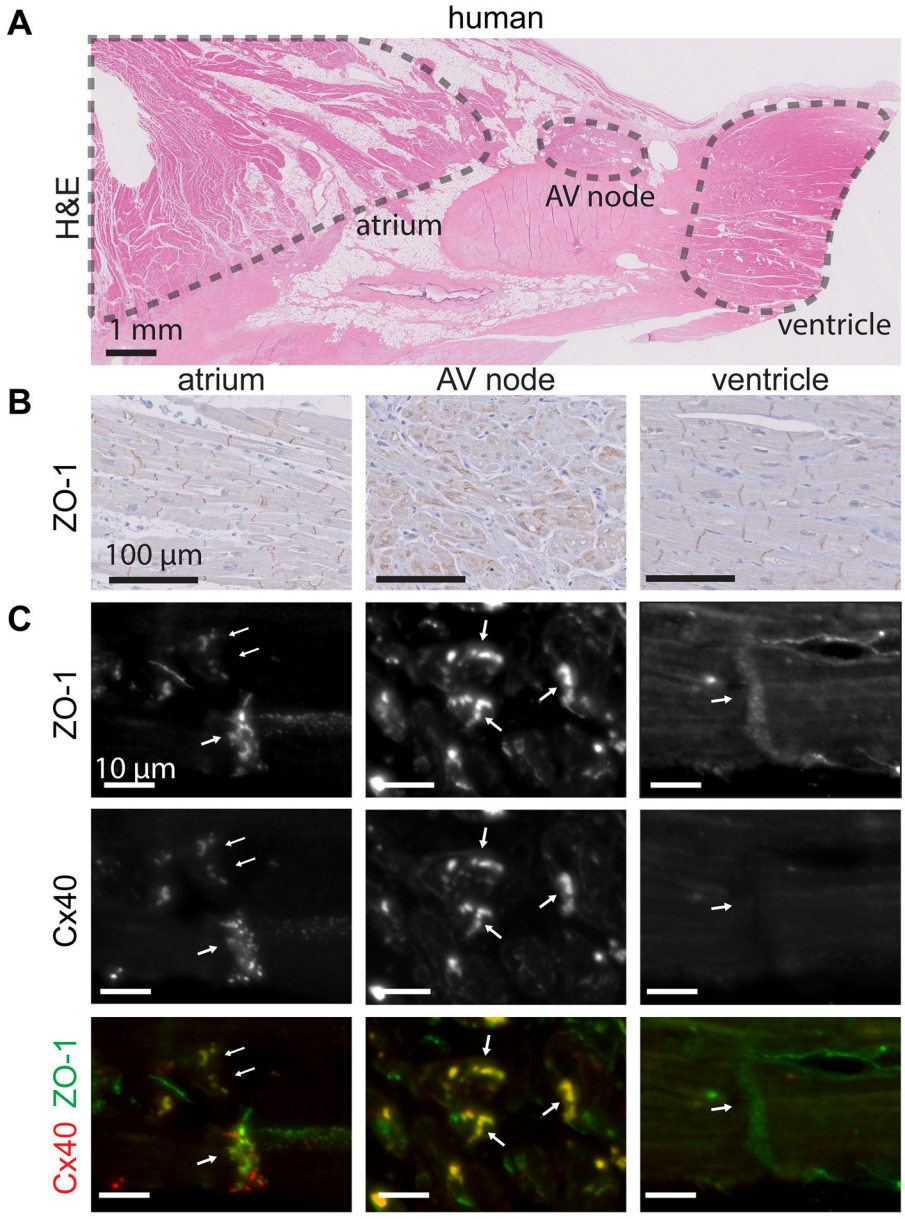

Figure 5: ZO-1 colocalizes with Cx40 in human AV nodes.

A. Representative H&E stain of a normal human AV node (scale bar=1 mm). B. Immunohistochemical staining of ZO-1 in normal human atrium, AV node, and ventricle (scale bar=100 µm). C. Immunofluorescence staining of ZO-1 and Cx40 in human atrium, AV node, and ventricle (scale bar=10 µm).

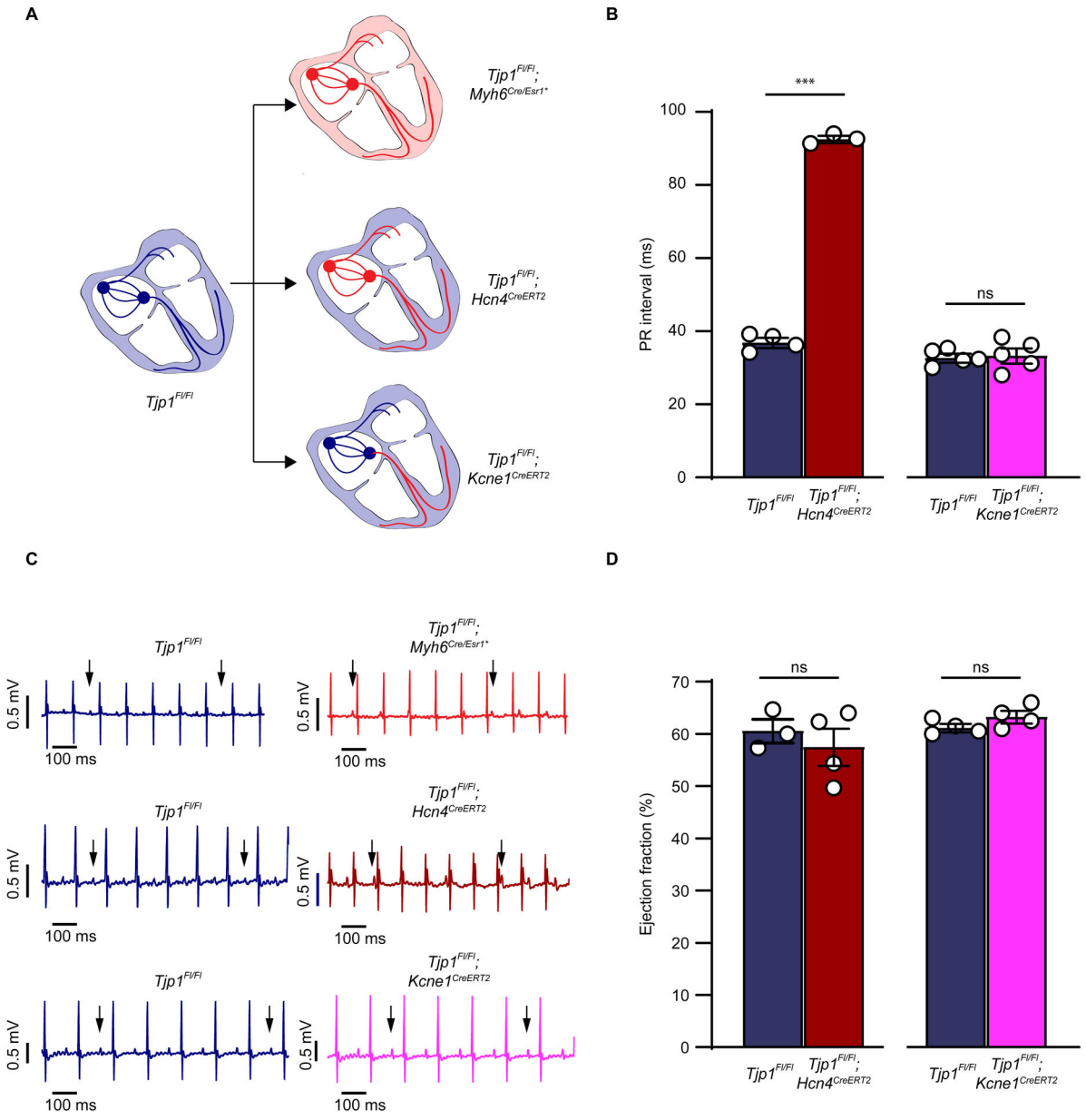

Figure 6: PR prolongation is due to ZO-1 loss proximal to the bundle of His.

A. Schematics of locations of ZO-1 deletion in *Tjp1*$^{fl/fl}$*; Myh6*$^{Cre/Esr1*}$, *Tjp1*$^{fl/fl}$*; Hcn4*^{CreERt2}, and *Tjp1*$^{fl/fl}$*; Kcne1*^{CreERt2} mouse lines. B. PR intervals of *Tjp1*$^{fl/fl}$*; Hcn4*^{CreERt2}, and *Tjp1*$^{fl/fl}$*; Kcne1*^{CreERt2} mice (p=2.7e-7, WRS: p=0.029, n=4 *Tjp1*$^{fl/fl}$ n=3 *Tjp1*$^{fl/fl}$*; Hcn4*^{CreERt2}). C. Representative surface ECG recordings in *Tjp1*$^{fl/fl}$*; Myh6*$^{Cre/Esr1*}$, *Tjp1*$^{fl/fl}$*; Hcn4*^{CreERt2}, and *Tjp1*$^{fl/fl}$*; Kcne1*^{CreERt2} mice (n=5 mice per genotype). D. Ejection fraction in *Tjp1*$^{fl/fl}$*; Hcn4*^{CreERt2}(p=0.51, n=3 *Tjp1*$^{fl/fl}$ n=4 *Tjp1*$^{fl/fl}$*; Hcn4*^{CreERt2} and *Tjp1*$^{fl/fl}$*; Kcne1*^{CreERt2} mice (p=0.1, n=4 mice per genotype). All studies were performed 10 d post-tamoxifen injection. (***p<0.001, ns indicates not significant). Two-tailed Student's t-test was used to calculate p-values.

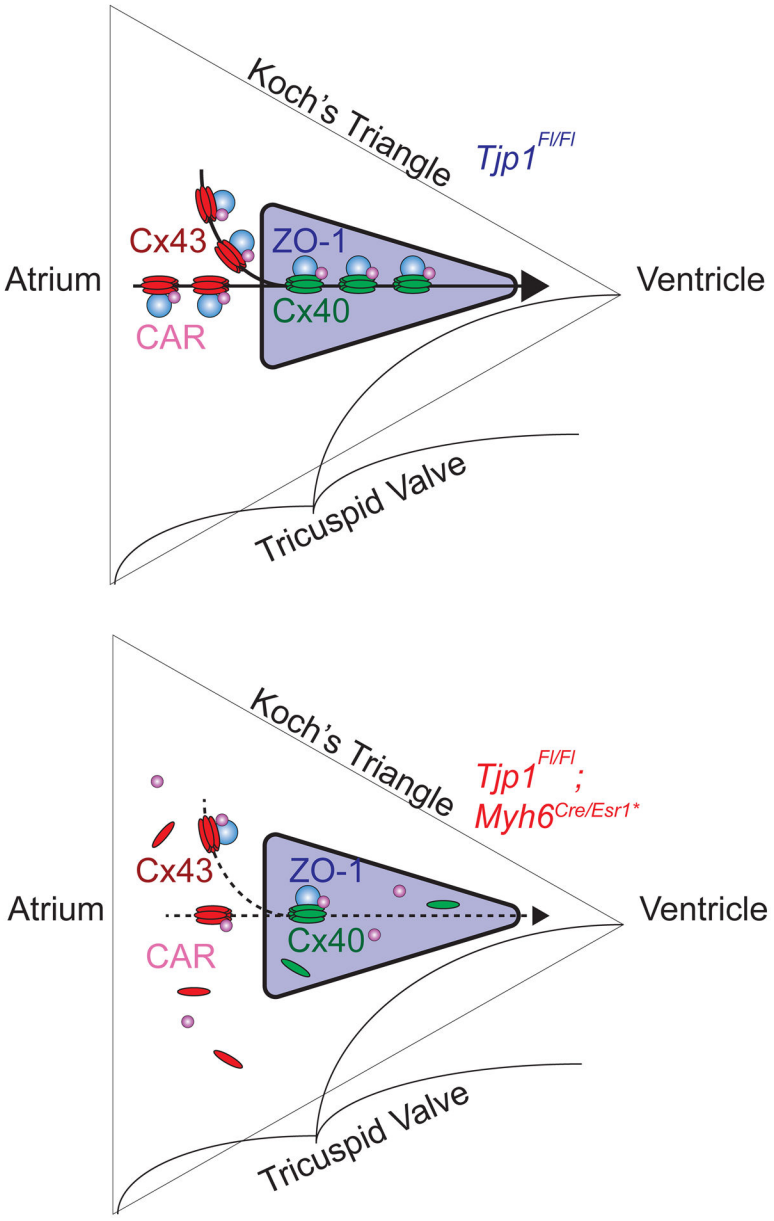

Figure 7: ZO-1 maintains AV nodal Cx40-ZO-1-CAR complex to facilitate atrial to ventricular conduction.

Electrical conduction from the atrium to ventricle passes through the AV node (purple triangle). A. Cx40-ZO-1-CAR protein complex exist at the cell-cell junctions within the AV node to maintain normal AV nodal conduction. B. When ZO-1 expression is lost in AV nodal cells, Cx40 and CAR cannot concentrate at cell-cell junctions, decreasing cell-cell conductance, leading to impeded AV nodal conduction (AV node purple, ZO-1 blue, Cx40 green, Cx43 red, CAR magenta).